

on the chip, and that were either associated with annotated Unigene 3' UTRs or represented in the expression atlas, as appropriate. Orthologous UTRs were aligned with ClustalW<sup>30</sup> using default parameters.

**Luciferase reporters**

Eight miR-1 targets were chosen randomly from those downregulated genes that possessed at least two 6-nt seed matches within a 1-kb segment of their 3' UTR. Two miR-124 targets were also selected, each of which contained two seed matches. Wild-type and mutant UTR segments were cloned into the 3' UTR of either a TK- or SV40-driven renilla luciferase-expressing plasmid, essentially as described<sup>3</sup>. Transfections were performed as previously<sup>9</sup>, except that 100 nM of miRNA duplex was transfected together with 5 ng of firefly luciferase reporter plasmid (transfection control), 1 µg of pUC19 plasmid (carrier), and either 250 ng of TK-renilla luciferase or 2 ng of SV40-renilla luciferase reporter plasmid. The cloned sequences and putative binding sites are described in the Supplementary Note. Relative luciferase values derived from cognate miRNA with wild-type plasmid cotransfections were compared (by Wilcoxon rank sum test), separately, to values from cognate miRNA with mutant plasmid, non-cognate miRNA with wild-type plasmid and non-cognate miRNA with mutant plasmid cotransfections.

**Expression atlas**

The human tissue expression atlas was described in the Supplementary Information of ref. 13, where the expression level of each gene is represented by the median intensity of its exon-exon junction probes. Because clustering analysis suggested that the intraventricular septum, pancreas and corpus callosum microarray samples had been mislabelled or mishybridized, these samples were not used in the analysis. Intensities that fell below 200 were not used to assign ranks, because they would be less than a standard deviation above the chip background signal; tissues that fell below this intensity were assigned the same ranks.

Received 22 July; accepted 22 December 2004; doi:10.1038/nature03315.  
Published online 30 January 2005.

1. Bartel, D. P. MicroRNAs: genomics, biogenesis, mechanism, and function. *Cell* **116**, 281–297 (2004).
2. Carrington, J. C. & Ambros, V. Role of microRNAs in plant and animal development. *Science* **301**, 336–338 (2003).
3. Lewis, B. P., Shih, I. H., Jones-Rhoades, M. W., Bartel, D. P. & Burge, C. B. Prediction of mammalian microRNA targets. *Cell* **115**, 787–798 (2003).
4. Palatnik, J. F. *et al.* Control of leaf morphogenesis by microRNAs. *Nature* **425**, 257–263 (2003).
5. Jackson, A. L. *et al.* Expression profiling reveals off-target gene regulation by RNAi. *Nature Biotechnol.* **21**, 635–637 (2003).
6. Hutvagner, G. & Zamore, P. D. A microRNA in a multiple-turnover RNAi enzyme complex. *Science* **297**, 2056–2060 (2002).
7. Zeng, Y., Yi, R. & Cullen, B. R. MicroRNAs and small interfering RNAs can inhibit mRNA expression by similar mechanisms. *Proc. Natl Acad. Sci. USA* **100**, 9779–9784 (2003).
8. Doench, J. G., Petersen, C. P. & Sharp, P. A. siRNAs can function as miRNAs. *Genes Dev.* **17**, 438–442 (2003).
9. Yekta, S., Shih, I. H. & Bartel, D. P. MicroRNA-directed cleavage of HOXB8 mRNA. *Science* **304**, 594–596 (2004).
10. Lagos-Quintana, M. *et al.* Identification of tissue-specific microRNAs from mouse. *Curr. Biol.* **12**, 735–739 (2002).
11. Sempere, L. F. *et al.* Expression profiling of mammalian microRNAs uncovers a subset of brain-expressed microRNAs with possible roles in murine and human neuronal differentiation. *Genome Biol.* **5**, R13 (2004).
12. Pruitt, K. D. & Maglott, D. R. RefSeq and LocusLink: NCBI gene-centered resources. *Nucleic Acids Res.* **29**, 137–140 (2001).
13. Johnson, J. M. *et al.* Genome-wide survey of human alternative pre-mRNA splicing with exon junction microarrays. *Science* **302**, 2141–2144 (2003).
14. Bailey, T. L. & Elkan, C. Fitting a mixture model by expectation maximization to discover motifs in biopolymers. *Proc. Int. Conf. Intell. Syst. Mol. Biol.* **2**, 28–36 (1994).
15. Lim, L. P. *et al.* The microRNAs of *Caenorhabditis elegans*. *Genes Dev.* **17**, 991–1008 (2003).
16. Wightman, B., Ha, I. & Ruvkun, G. Posttranscriptional regulation of the heterochronic gene lin-14 by lin-4 mediates temporal pattern formation in *C. elegans*. *Cell* **75**, 855–862 (1993).
17. Lai, E. C. Micro RNAs are complementary to 3' UTR sequence motifs that mediate negative post-transcriptional regulation. *Nature Genet.* **30**, 363–364 (2002).
18. Doench, J. G. & Sharp, P. A. Specificity of microRNA target selection in translational repression. *Genes Dev.* **18**, 504–511 (2004).
19. John, B. *et al.* Human MicroRNA targets. *PLoS Biol.* **2**, e363 (2004).
20. Rhoades, M. W. *et al.* Prediction of plant microRNA targets. *Cell* **110**, 513–520 (2002).
21. Haley, B. & Zamore, P. D. Kinetic analysis of the RNAi enzyme complex. *Nature Struct. Mol. Biol.* **11**, 599–606 (2004).
22. Martinez, J. & Tuschl, T. RISC is a 5' phosphomonoester-producing RNA endonuclease. *Genes Dev.* **18**, 975–980 (2004).
23. Janz, R. & Sudhof, T. C. Cellugyrin, a novel ubiquitous form of synaptogyrin that is phosphorylated by pp60c-src. *J. Biol. Chem.* **273**, 2851–2857 (1998).
24. Vartiainen, M. K., Sarkkinen, E. M., Matilainen, T., Salminen, M. & Lappalainen, P. Mammals have two twinfilin isoforms whose subcellular localizations and tissue distributions are differentially regulated. *J. Biol. Chem.* **278**, 34347–34355 (2003).
25. Bartel, D. P. & Chen, C. Z. Micromanagers of gene expression: the potentially widespread influence of metazoan microRNAs. *Nature Rev. Genet.* **5**, 396–400 (2004).
26. Ashburner, M. *et al.* Gene ontology: tool for the unification of biology. The Gene Ontology Consortium. *Nature Genet.* **25**, 25–29 (2000).
27. Schwarz, D. S. *et al.* Asymmetry in the assembly of the RNAi enzyme complex. *Cell* **115**, 199–208 (2003).
28. Khvorova, A., Reynolds, A. & Jayasena, S. D. Functional siRNAs and miRNAs exhibit strand bias. *Cell* **115**, 209–216 (2003).

29. Hughes, T. R. *et al.* Functional discovery via a compendium of expression profiles. *Cell* **102**, 109–126 (2000).
30. Thompson, J. D., Higgins, D. G. & Gibson, T. J. CLUSTAL W: improving the sensitivity of progressive multiple sequence alignment through sequence weighting, position-specific gap penalties and weight matrix choice. *Nucleic Acids Res.* **22**, 4673–4680 (1994).

Supplementary Information accompanies the paper on [www.nature.com/nature](http://www.nature.com/nature).

**Acknowledgements** Thanks to S. Baskerville, M. Cleary and P. Sharp for comments on the manuscript, C. Armour, S. Bartz, J. Burchard, G. Cavet, D. Haynor, A. Jackson, M. Pellegrini, E. Schadt and Y. Wang for their assistance, the Rosetta Gene Expression Laboratory for microarray work, M. Jones-Rhoades for primer design, and W. Johnston for plasmid construction.

**Competing interests statement** The authors declare that they have no competing financial interests.

**Correspondence** and requests for materials should be addressed to L.P.L. ([lee\\_lim@merck.com](mailto:lee_lim@merck.com)). The GEO accession number for the microarray data is GSE2075.

.....  
**Highly coupled ATP synthesis by F<sub>1</sub>-ATPase single molecules**

**Yannick Rondelez<sup>1,2</sup>, Guillaume Tresset<sup>1,2</sup>, Takako Nakashima<sup>2</sup>, Yasuyuki Kato-Yamada<sup>3</sup>, Hiroyuki Fujita<sup>4</sup>, Shoji Takeuchi<sup>4</sup> & Hiroyuki Noji<sup>2</sup>**

<sup>1</sup>LIMMS/CNRS-IIS, <sup>2</sup>Institute of Industrial Science, The University of Tokyo, Tokyo 153-8505, Japan  
<sup>3</sup>Department of Life Science, College of Science, Rikkyo (St Paul's) University, Tokyo 171-8501, Japan  
<sup>4</sup>CIRMM, Institute of Industrial Science, The University of Tokyo, Tokyo 153-8505, Japan

F<sub>1</sub>-ATPase is the smallest known rotary motor, and it rotates in an anticlockwise direction as it hydrolyses ATP<sup>1–3</sup>. Single-molecule experiments<sup>6–9</sup> point towards three catalytic events per turn, in agreement with the molecular structure of the complex<sup>10</sup>. The physiological function of F<sub>1</sub> is ATP synthesis. In the ubiquitous F<sub>0</sub>F<sub>1</sub> complex, this energetically uphill reaction is driven by F<sub>0</sub>, the partner motor of F<sub>1</sub>, which forces the backward (clockwise) rotation of F<sub>1</sub>, leading to ATP synthesis<sup>11–13</sup>. Here, we have devised an experiment combining single-molecule manipulation and microfabrication techniques to measure the yield of this mechanochemical transformation. Single F<sub>1</sub> molecules were enclosed in femtolitre-sized hermetic chambers and rotated in a clockwise direction using magnetic tweezers. When the magnetic field was switched off, the F<sub>1</sub> molecule underwent anticlockwise rotation at a speed proportional to the amount of synthesized ATP. At 10 Hz, the mechanochemical coupling efficiency was low for the α<sub>3</sub>β<sub>3</sub>γ subcomplex (F<sub>1</sub><sup>ε</sup>), but reached up to 77% after reconstitution with the ε-subunit (F<sub>1</sub><sup>ε+</sup>). We provide here direct evidence that F<sub>1</sub> is designed to tightly couple its catalytic reactions with the mechanical rotation. Our results suggest that the ε-subunit has an essential function during ATP synthesis.

Genetically engineered, single F<sub>1</sub> molecules can be grafted on to a glass slide, and the ATP-driven anticlockwise rotation has been observed directly under an optical microscope by coupling the γ-subunit to a fluorescent filament or a submicrometre-sized plastic bead<sup>9,14</sup>. Our experiment used a similar procedure with some alternations: the magnetic bead was attached to the γ-subunit to rotate it relative to the glass-bound α<sub>3</sub>β<sub>3</sub> stator part of the F<sub>1</sub> molecule using magnetic tweezers<sup>15</sup>. We also developed a microfabrication technique to confine this system to a 6-fl transparent container<sup>16</sup> (Fig. 1b). Owing to the extremely small volume, the number of ATP molecules produced by a single F<sub>1</sub> enzyme reached a

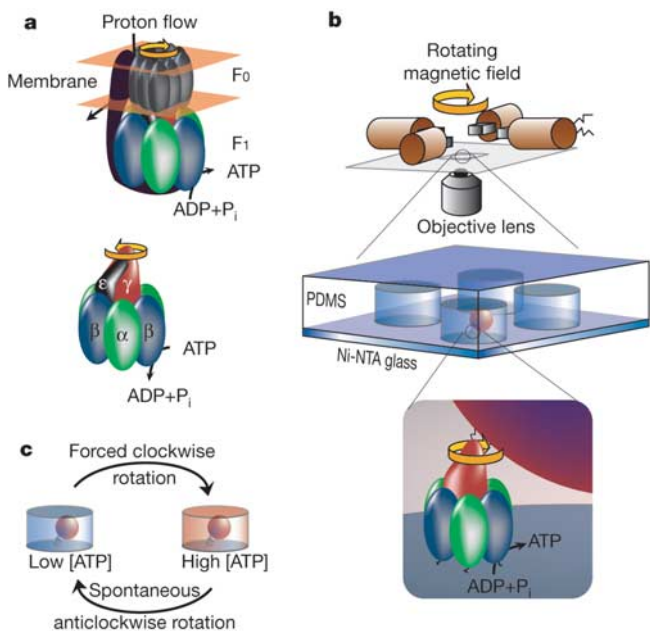


**Figure 1** ATP synthesis by  $F_1$ -ATPase. **a**, Schematic view of the membrane-embedded  $F_0F_1$ -ATP synthase in which the proton-driven  $F_0$  rotates  $F_1$  in a clockwise direction for ATP synthesis. Isolated  $F_1$  only hydrolyses ATP, and hence is called  $F_1$ -ATPase.  $F_1$ -ATPase comprises five different subunits,  $\alpha_3\beta_3\gamma\delta\epsilon$ , of which the  $\alpha_3\beta_3\gamma$  subcomplex is the minimal functional part of the ATPase<sup>30</sup>. ATP hydrolysis occurs sequentially on the three  $\beta$ -subunits, which generate power strokes driving the anticlockwise rotation of  $\gamma\epsilon$  (or  $\gamma$  if  $\epsilon$  is absent). **b**, To force the ATP synthesis of  $F_1$  against the chemical potential, a magnetic bead was attached to the  $\gamma$ -subunit of an immobilized  $F_1$ , and rotated clockwise using magnetic tweezers. A single bead–enzyme complex was enclosed in a PDMS container in order to trap synthesized ATP molecules. **c**, ATP synthesis was detectable via the enzyme itself: after the magnetic field was released, the enzyme resumed its ATP-hydrolysing anticlockwise rotation at a speed proportional to the ATP concentration in the chamber.

detectable micromolar concentration within minutes of forced clockwise rotation. After the magnetic field was switched off, this ATP concentration could be readily determined by monitoring the speed of the enzyme spontaneously rotating in an anticlockwise direction. By comparing the number of turns in both directions (mechanical input/output) with the changes in ATP concentration (chemical input/output), we were able to assess directly the mechanochemical coupling efficiencies of  $F_1$ .

As a first step, we focused on the enzyme acting as a motor; that is, hydrolysing ATP.  $F_1$  molecules were immobilized on a glass plate at a density of less than one per  $4 \mu\text{m}^2$  (the surface area of a chamber). A polydimethylsiloxane (PDMS) sheet with microchambers on its surface (Fig. 2a, left) was suspended above the glass plate and partially pressed down onto it with a small, flat-tipped glass needle to enclose a rotating  $F_1$  molecule in a chamber (Fig. 2b). The chamber size was large enough to avoid physical conflict with the rotating bead (Fig. 2a, right), and could contain only  $1,800 \pm 200$  ATP molecules at 500 nM ATP. (The error number was derived from the error of the chamber volume, around 10%.) Because the motor consumed ATP molecules in the chamber, the rotation speed decreased (Fig. 2c). Under these conditions of low ATP concentration, where ATP binding is the rate-limiting step, the speed decreases linearly with ATP concentration and the expected first-order decay was observed (Fig. 2d). We re-opened the chamber when the speed approached zero, thus taking back the system to its initial condition (Fig. 2b). The enzyme immediately resumed its initial speed, showing that the motor was still active. Extrapolating the rotation speed versus the number of accumulated rotations (Fig. 2d, inset) yielded the maximum number of turns that the single enzyme could perform by exhausting the 1,800 available ATP molecules. We determined the value to be  $580 \pm 100$  turns (mean  $\pm$  s.d.), corresponding to a coupling ratio of  $3.15 \pm 0.5$  ATPs per turn. A similar result was obtained for  $F_1^{+\epsilon}$  (data not shown). Such a high coupling ratio in the motor direction had been proposed previously<sup>8,17</sup>, but only indirect evidence had been provided so far, because the mechanical output and the real ATP

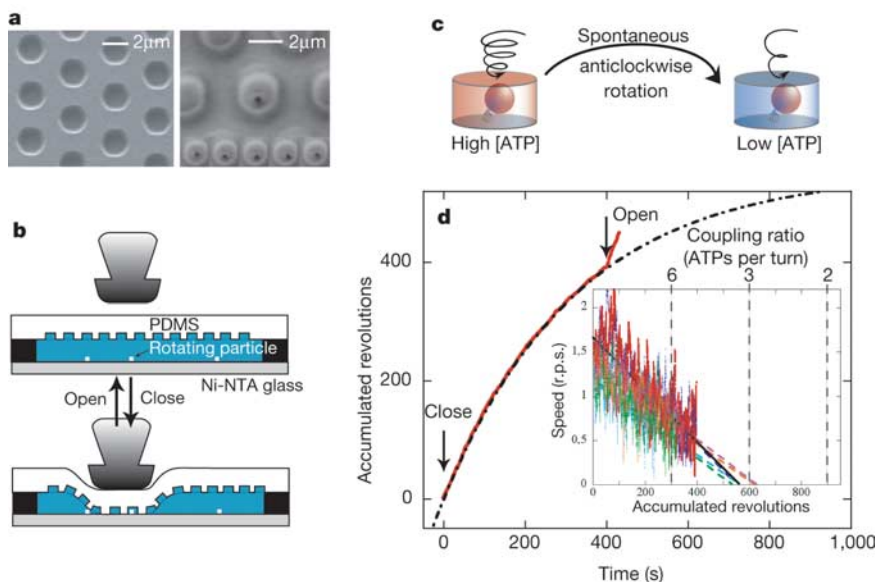


**Figure 2** Determination of the coupling efficiency of ATP hydrolysis. **a**, Scanning electron microscopy image of a PDMS sheet with cylindrical cavities of 1.1- $\mu\text{m}$  radius and 1.5- $\mu\text{m}$  height (left), and a bright-field image under an optical microscope after enclosing a rotating bead (right), with successive images of rotation. **b**, Elastic properties of PDMS allow the reversible closing/opening of the chamber, by partially pressing a suspended sheet against the bottom glass plate. **c**, The chamber volume was small enough to ensure that a single enzyme exhausted most of the available ATP (1,800 molecules) within a few

minutes. **d**, Time course of accumulated revolutions showing an exponential decay after closing the chamber, and the recovery of the initial velocity after opening the chamber. The inset shows the rotation speeds as a function of the accumulated revolutions for six different  $F_1$  molecules. The linear decreases were extrapolated to give the maximum number of possible turns and the coupling ratio between ATP hydrolysis and mechanical rotation.

consumption could not be monitored simultaneously. In particular, the possibility that the motor might 'slip' and hydrolyse ATP without rotation was a lingering question. Back steps<sup>8</sup> could also affect the coupling ratio; however, this was such a rare event (less than 1% in our case) that it can be considered to be negligible. The present experiment directly demonstrates that  $F_1^{+e}$  and  $F_1^{-e}$  do not waste ATP, and work as motors with nearly perfect mechanochemical coupling efficiencies.

In a second series of experiments, we turned to the more challenging question of ATP synthesis. The buffer now included physiological concentrations of ADP and inorganic phosphate  $P_i$ , as well as 200 nM ATP, in order to identify active rotating molecules. As before, the chamber was closed around a single enzyme, but its rotation was now forced into the clockwise direction using a

rotating magnetic field and the magnetic bead as a handle. The maximum rate of ATP synthesis for this thermophilic  $F_0F_1$  enzyme was biochemically determined to be  $30 \text{ ATPs s}^{-1}$  at room temperature (R. Iino and M. Yoshida, personal communication). Therefore, we selected a rotating speed of 10 rotations per second (r.p.s.). The magnetic field was applied in repetitive sequences of 1 min duration, with an interval of  $\sim 1 \text{ min}$  (Fig. 3a, b). When it was turned off, the bead resumed its anticlockwise rotation at a speed proportional to the ATP concentration.

If perfect mechanical coupling is assumed, the enzyme should produce three ATPs per clockwise turn. The concentration increment after 10 Hz rotation for 1 min corresponds to 500 nM ATP in 6 fl. This is a significantly higher concentration than the initial ATP concentration of 200 nM, thus one would expect a marked

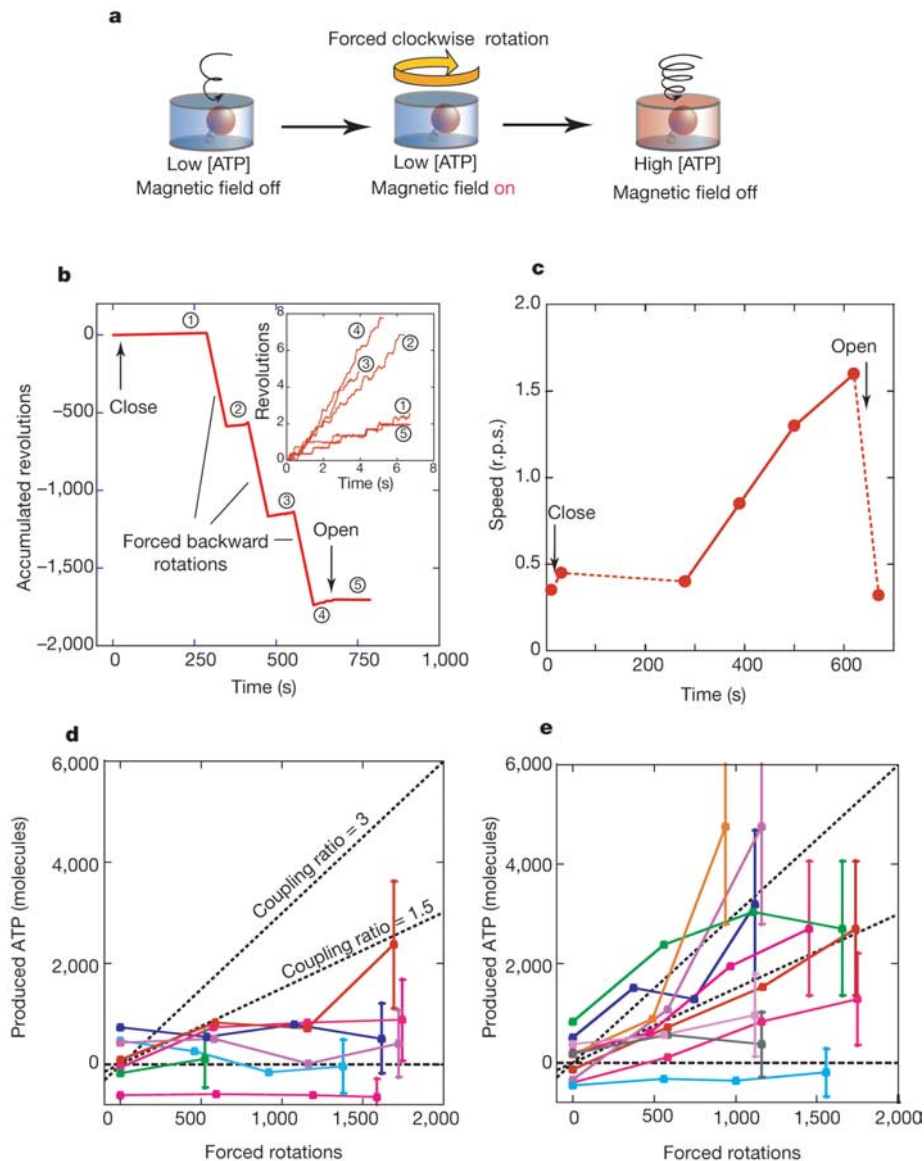


**Figure 3** Determination of the coupling efficiency of ATP synthesis. **a, b**, An  $F_1^{-e/+e}$  enzyme bound to a magnetic bead was rotated in a backward (clockwise) direction with magnetic tweezers within a microchamber in the presence of ADP,  $P_i$  and a small amount of ATP. Synthesized ATP accumulated in the chamber. Before and after a forced clockwise rotation, spontaneous anticlockwise rotation was recorded as a means of detecting ATP synthesis through the increased rotational speed (see inset). **c**, The anticlockwise rotation speeds at each experimental step in **a** are shown. Between the second and third point, the

motor was stalled without rotation in order to confirm the absence of background ATP synthesis. **d, e**, Anticlockwise rotation speeds were converted into the total number of synthesized ATPs for  $F_1^{-e}$  (**d**) and  $F_1^{+e}$  (**e**). Each trace belongs to an individual  $F_1$  molecule. Dotted lines indicate ATP yields expected for mechanochemical coupling ratios: 3 for 100% efficiency; 1.5 for 50%; and 0 for 0%. The standard error deviation from the rotational velocity determination (30%) and the chamber volume (10%) is indicated at each end of the traces only, for the sake of clarity.

acceleration of the anticlockwise rotation after release of the magnetic field. Notably, this was not the case for  $F_1^{-\epsilon}$ : the beads hardly increased their speed. Analysis of these experiments (Fig. 3d) gave a coupling ratio of  $0.5 \pm 0.4$  (mean  $\pm$  s.d.) ATPs produced per turn. This is in agreement with a previous bulk experiment<sup>13</sup>, indicating a very low mechanochemical coupling efficiency of  $F_1^{-\epsilon}$  at 10 Hz.

The results were different for  $F_1^{+\epsilon}$ , reconstituted from  $F_1^{-\epsilon}$  and the  $\epsilon$ -subunit. In this case, the forced backward rotations led, in most experiments, to a large increase in the rotation speed (Fig. 3b, c). These reproducible patterns confirmed the production of ATP inside the microchamber. For computation of the ATP yield from the rotation speed, calibration curves of the speed versus ATP concentration (ranging from 200 nM to 2 mM) were determined in independent experiments in the same buffer (see Supplementary Information). It followed Michaelis–Menten kinetics. We then calculated the number of ATP molecules produced from the increment of ATP concentration and the chamber volume to compare with the number of forced clockwise rotations (Fig. 3e). Most traces were found between dotted lines for coupling ratios of 3 and 1.5. We obtained an average value of  $2.3 \pm 1.6$  (mean  $\pm$  s.d.) ATPs per turn (77%) after eliminating obviously defective traces (blue and grey traces in Fig. 3e). This is probably a lower limit, because most artefacts, such as transient leaks in the chamber, defective connections in the glass– $F_1$ –streptavidin–bead complex, or contamination by other free motors, should decrease this value. Therefore our data point to an excellent mechanochemical coupling efficiency. In the best cases, we observed the postulated value of three ATPs synthesized per turn.

Efficiency of molecular machines is generally difficult to assess because it requires precise mechanical information—available only at the single-molecule level—while simultaneously measuring minute amounts of chemical output<sup>17</sup>. Moreover, it is easier to detect a mechanical output from a chemical input than to do the contrary. The mechanical synthesis of ATP by reversing  $F_1$  molecules was previously reported<sup>13</sup>, but it was not a quantitative measurement. As a consequence, a good understanding of the ATP-hydrolysing function of  $F_1$  has been accumulated<sup>1,3,4</sup>, but very little was known about its biologically more relevant ATP synthesis ability<sup>2</sup>. In this approach we have taken advantage of transparent containers so small that a single enzyme's chemical activity quickly results in detectable concentration changes<sup>16</sup>. Our experiments show that both  $F_1^{-\epsilon}$  and  $F_1^{+\epsilon}$  consume strictly three ATPs per anticlockwise turn, whereas only  $F_1^{+\epsilon}$  is efficient enough to produce ATP when forced to rotate in the backward (clockwise) direction. These results are consistent with the ubiquity of this strategic enzyme that fuels most of the energy-consuming biological processes.

The present work reveals the unexpected importance of the  $\epsilon$ -subunit in the synthesis of ATP. Its regulatory role for ATP hydrolysis is well recognized<sup>18–20</sup> but its exact function in synthesis is still a matter for discussion. Our findings suggest that the  $\epsilon$ -subunit is necessary for high-yield and high-rate ATP synthesis. It was already known that the absence of the  $\epsilon$ -subunit suppresses the synthesizing ability of chloroplast  $F_0F_1$ <sup>21</sup>, even though the enzyme is structurally intact. Recent biochemical studies have suggested that  $\epsilon$  can insert its helical domain into the  $\alpha_3\beta_3$  ring, in a cleft along the  $\gamma$ -subunit<sup>22–24</sup>. This could be the structural basis for a switch of the enzyme into the ATP synthesis mode<sup>23</sup>, and/or a shift in the ATP/ADP affinity balance<sup>2</sup>. Alternatively, as shown in the crystal structure<sup>25</sup> of  $F_1^{+\epsilon}$ , the  $\epsilon$ -subunit may stabilize the protruding part of the  $\gamma$ -subunit where the mechanical torque is applied. In this case, it would possess mostly a structural function. The precise role of the  $\epsilon$ -subunit in ATP synthesis remains to be established. The experimental set-up described here can also be used to investigate the parameters of the original mechanical-to-chemical biological transduction performed by  $F_1$ , such as maximum velocity, torque, energy barriers and affinities for substrates. □

## Methods

### Materials

All buffers were prepared with 0.05 mg ml<sup>-1</sup> heat-shock-purified BSA, 50 mM MOPS pH 7, 50 mM KCl and 2 mM MgCl<sub>2</sub>. For the ATP-driven rotation assay, 500 nM ATP was added, whereas for ATP synthesis the buffer contained 200 nM ATP, 10 mM P<sub>i</sub> and 100  $\mu$ M ADP, which was purified as previously described<sup>13</sup>. In buffers containing both BSA and ADP, spontaneous ATP synthesis activity was detected owing to contaminating adenylate kinase in BSA. However, the activity was negligible, less than 2 nM h<sup>-1</sup>. A mutant  $F_1^{+\epsilon}$  (His<sub>6</sub>- $\alpha$ C193S, His<sub>10</sub>- $\beta$  and  $\gamma$ S107C/I210C), derived from the thermophilic *Bacillus* PS3, was prepared and biotinylated as described<sup>26</sup>. Six His tags were used to strengthen the binding of  $F_1$  to the glass plate, but did not alter significantly the rotary and catalytic properties of  $F_1$  as compared to previous mutants<sup>9</sup>. Recombinant  $\epsilon$ -subunit was prepared as described<sup>7</sup> and mixed at 7.5  $\mu$ M with 0.5  $\mu$ M  $F_1^{-\epsilon}$ , in order to reconstitute  $F_1^{+\epsilon}$ . PDMS sheets with microchambers were prepared by conventional moulding procedures<sup>27</sup> with a slight modification<sup>16</sup>. The dimensions of the chambers, determined from electron microscope images, were 1.13  $\mu$ m radius and 1.50  $\mu$ m height, with an average volume of 6.0  $\pm$  0.6 fl (mean  $\pm$  s.d.).

### Equipment

The magnetic field was generated by custom-made magnetic tweezers<sup>15</sup> mounted on the stage of a microscope (Olympus, IX71). The bead rotation was recorded using a CCD camera (MTI, RC300) at the video rate, and the trajectories of rotation were analysed using custom-made software (R. Yasuda). During the time intervals when the magnetic field was cut off, the speed of ATP-driven rotation was calculated from more than five successive turns<sup>28</sup>.

### ATP-driven rotation assay in a chamber

A 2  $\times$  20 mm<sup>2</sup> flow cell was constructed by suspending a PDMS sheet on top of a Ni-NTA-modified cover plate with two 40- $\mu$ m spacer sheets.  $F_1$  molecules were immobilized on the cover plate at a very low concentration (4.7 pM), such that the density of immobilized  $F_1$  was less than one enzyme per 4  $\mu$ m<sup>2</sup> (the surface of a chamber). Streptavidin-coated magnetic beads (Seradyn;  $\sim$ 0.47- $\mu$ m diameter) were then attached to the biotinylated  $\gamma$ -subunit. When a rotating bead was found, it was enclosed in a microchamber by pressing down on the PDMS sheet using a glass needle (30- $\mu$ m diameter) controlled by a z-axis micromanipulator (Narishige). After visual confirmation of contact between the sheet and the cover plate, the glass needle was pressed down a further 2–3  $\mu$ m to seal the chambers tightly. This value is less than 10% of the value required for the complete compression (more than 30  $\mu$ m). Thus, taking the elastomeric properties of PDMS<sup>29</sup> into account, the chamber volume was not strongly modified under these conditions; this is also supported by the ATP-driven rotation experiments. On rare occasions, small focus drifts and transient leakage of the chamber were observed, in which case the entire experiment was rejected.

### Mechanical ATP synthesis in a chamber

The set-up was similar to previous experiments, but magnetic tweezers and synthesis buffer were used. Under these high ADP conditions, more than 90% of  $F_1^{-\epsilon}$  or  $F_1^{+\epsilon}$  molecules were in the Mg-ADP-inhibited form (data not shown). Therefore, most of the magnetic beads did not show rotation, and they had to be pushed into the active state by mechanical, 180° clockwise rotation<sup>15</sup>. A 10 Hz rotating magnetic field was applied for 1 min to force 600 turns in the clockwise direction. Some beads (possibly with a lower magnetic content) did not perfectly follow the rotating field, and thus the actual number of clockwise turns had to be directly counted from the video analysis. Between rounds of the forced rotation, speed of the ATP-driven anticlockwise rotation was measured. The standard curves (see Supplementary Information) were built from independent experiments in regular flow cells. Michaelis–Menten parameters ( $F_1^{-\epsilon}$ :  $K_m = 3.3$   $\mu$ M,  $V_{max} = 4.5$  r.p.s.;  $F_1^{+\epsilon}$ :  $K_m = 2.1$   $\mu$ M,  $V_{max} = 4.9$  r.p.s.) and the chamber volumes were used to convert rotational speed into the total number of synthesized ATP molecules.

Received 17 August; accepted 8 December 2004; doi:10.1038/nature03277.

- Boyer, P. D. The ATP synthase—a splendid molecular machine. *Annu. Rev. Biochem.* **66**, 717–749 (1997).
- Senior, A. E., Nadanaciva, S. & Weber, J. The molecular mechanism of ATP synthesis by  $F_1F_0$ -ATP synthase. *Biochim. Biophys. Acta* **1553**, 188–211 (2002).
- Yoshida, M., Muneyuki, E. & Hisabori, T. ATP synthase—a marvellous rotary engine of the cell. *Nature Rev. Mol. Cell Biol.* **2**, 669–677 (2001).
- Kinosita, K. Jr, Yasuda, R. & Noji, H.  $F_1$ -ATPase: a highly efficient rotary ATP machine. *Essays Biochem.* **35**, 3–18 (2000).
- Leslie, A. G. & Walker, J. E. Structural model of  $F_1$ -ATPase and the implications for rotary catalysis. *Phil. Trans. R. Soc. Lond. B* **355**, 465–471 (2000).
- Noji, H., Yasuda, R., Yoshida, M. & Kinosita, K. Jr Direct observation of the rotation of  $F_1$ -ATPase. *Nature* **386**, 299–302 (1997).
- Kato-Yamada, Y., Noji, H., Yasuda, R., Kinosita, K. Jr & Yoshida, M. Direct observation of the rotation of  $\epsilon$  subunit in  $F_1$ -ATPase. *J. Biol. Chem.* **273**, 19375–19377 (1998).
- Yasuda, R., Noji, H., Kinosita, K. Jr & Yoshida, M.  $F_1$ -ATPase is a highly efficient molecular motor that rotates with discrete 120 degree steps. *Cell* **93**, 1117–1124 (1998).
- Yasuda, R., Noji, H., Yoshida, M., Kinosita, K. Jr & Itoh, H. Resolution of distinct rotational substeps by submillisecond kinetic analysis of  $F_1$ -ATPase. *Nature* **410**, 898–904 (2001).
- Abrahams, J. P., Leslie, A. G., Lutter, R. & Walker, J. E. Structure at 2.8 Å resolution of  $F_1$ -ATPase from bovine heart mitochondria. *Nature* **370**, 621–628 (1994).
- Zhou, Y., Duncan, T. M. & Cross, R. L. Subunit rotation in *Escherichia coli*  $F_0F_1$ -ATP synthase during oxidative phosphorylation. *Proc. Natl Acad. Sci. USA* **94**, 10583–10587 (1997).

12. Diez, M. *et al.* Proton-powered subunit rotation in single membrane-bound  $F_0F_1$ -ATP synthase. *Nature Struct. Mol. Biol.* **11**, 135–141 (2004).
13. Itoh, H. *et al.* Mechanically driven ATP synthesis by  $F_1$ -ATPase. *Nature* **427**, 465–468 (2004).
14. Hirono-Hara, Y. *et al.* Pause and rotation of  $F_1$ -ATPase during catalysis. *Proc. Natl Acad. Sci. USA* **98**, 13649–13654 (2001).
15. Hirono-Hara, Y. *et al.* Activation of pausing  $F_1$ -motor by external force. *Proc. Natl Acad. Sci. USA*. (in the press).
16. Rondelez, Y. *et al.* Microfabricated array of femtoliter chambers allow single molecule enzymology. *Nature Biotechnol.* (in the press).
17. Nishizaka, T. *et al.* Chemomechanical coupling in  $F_1$ -ATPase revealed by simultaneous observation of nucleotide kinetics and rotation. *Nature Struct. Mol. Biol.* **11**, 142–148 (2004).
18. Laget, P. P. & Smith, J. B. Inhibitory properties of endogenous subunit  $\epsilon$  in the *Escherichia coli*  $F_1$  ATPase. *Arch. Biochem. Biophys.* **197**, 83–89 (1979).
19. Dunn, S. D., Zadorozny, V. D., Tozer, R. G. & Orr, L. E. Epsilon subunit of *Escherichia coli*  $F_1$ -ATPase: effects on affinity for aurovertin and inhibition of product release in unisite ATP hydrolysis. *Biochemistry* **26**, 4488–4493 (1987).
20. Kato, Y. *et al.* Thermophilic  $F_1$ -ATPase is activated without dissociation of an endogenous inhibitor,  $\epsilon$  subunit. *J. Biol. Chem.* **272**, 24906–24912 (1997).
21. Nowak, K. F., Tabidze, V. & McCarty, R. E. The C-terminal domain of the  $\epsilon$  subunit of the chloroplast ATP synthase is not required for ATP synthesis. *Biochemistry* **41**, 15130–15134 (2002).
22. Tsunoda, S. P. *et al.* Large conformational changes of the  $\epsilon$  subunit in the bacterial  $F_1F_0$  ATP synthase provide a ratchet action to regulate this rotary motor enzyme. *Proc. Natl Acad. Sci. USA* **98**, 6560–6564 (2001).
23. Suzuki, T. *et al.*  $F_0F_1$ -ATPase/synthase is geared to the synthesis mode by conformational rearrangement of  $\epsilon$  subunit in response to proton motive force and ADP/ATP balance. *J. Biol. Chem.* **278**, 46840–46846 (2003).
24. Bulygin, V. V., Duncan, T. M. & Cross, R. L. Rotor/stator interactions of the  $\epsilon$  subunit in *Escherichia coli* ATP synthase and implications for enzyme regulation. *J. Biol. Chem.* **279**, 35616–35621 (2004).
25. Gibbons, C., Montgomery, M. G., Leslie, A. G. & Walker, J. E. The structure of the central stalk in bovine  $F_1$ -ATPase at 2.4 Å resolution. *Nature Struct. Biol.* **7**, 1055–1061 (2000).
26. Noji, H. *et al.* Purine but not pyrimidine nucleotides support rotation of  $F_1$ -ATPase. *J. Biol. Chem.* **276**, 25480–25486 (2001).
27. McDonald, J. C. & Whitesides, G. M. Poly(dimethylsiloxane) as a material for fabricating microfluidic devices. *Acc. Chem. Res.* **35**, 491–499 (2002).
28. Adachi, K., Noji, H. & Kinoshita, K. Jr Single-molecule imaging of rotation of  $F_1$ -ATPase. *Methods Enzymol.* **361**, 211–227 (2003).
29. Unger, M. A., Chou, H. P., Thorsen, T., Scherer, A. & Quake, S. R. Monolithic microfabricated valves and pumps by multilayer soft lithography. *Science* **288**, 113–116 (2000).
30. Matsui, T. & Yoshida, M. Expression of the wild-type and the Cys-Trp-less  $\alpha_3\beta_3\gamma$  complex of thermophilic  $F_1$ -ATPase in *Escherichia coli*. *Biochim. Biophys. Acta* **1231**, 139–149 (1995).

Supplementary Information accompanies the paper on [www.nature.com/nature](http://www.nature.com/nature).

**Acknowledgements** We thank all members of the Noji and Takeuchi laboratories, and H. Arata and A. Tixier-Mita for discussion and experimental support; R. Yasuda for PC programming of image analysis (CREST image); and Central Workshop in IIS for an optical microscope stage. This work was performed in the framework of LIMMS/CNRS-IIS, and supported in part by Bio-oriented Technology Research Advancement Institution (H.N. and S.T.), and Grants-in-Aid from Ministry of Education, Science, Sports and Culture of Japan (H.N., H.F. and S.T.). Y.R. and G.T. are Research Fellows of the Japan Society for the Promotion of Science.

**Competing interests statement** The authors declare that they have no competing financial interests.

**Correspondence** and requests for materials should be addressed to H.N. (hnoji@iis.u-tokyo.ac.jp).

.....  
**corrigendum**

**Sequence and comparative analysis of the chicken genome provide unique perspectives on vertebrate evolution**

**International Chicken Genome Sequencing Consortium**

*Nature* **432**, 695–716 (2004).

In Table 5 of this Article, the last four values listed in the ‘Copy number’ column were incorrect. These should be: LTR elements, 30,000; DNA transposons, 20,000; simple repeats, 140,000; and satellites, 4,000. These errors do not affect any of the conclusions in our paper. □